

SYNAPSE: Framework for Neuron Analysis and Perturbation in Sequence Encoding

Jesús Sánchez Ochoa^a, Enrique Tomás Martínez Beltrán^{a,*}, Alberto Huertas Celdrán^a

^a*Department of Information and Communications Engineering, University of Murcia, Murcia, 30100, Spain*

Abstract

In recent years, Artificial Intelligence has become a powerful partner for complex tasks such as data analysis, prediction, and problem-solving, yet its lack of transparency raises concerns about its reliability. In sensitive domains such as healthcare or cybersecurity, ensuring transparency, trustworthiness, and robustness is essential, since the consequences of wrong decisions or successful attacks can be severe. Prior neuron-level interpretability approaches are primarily descriptive, task-dependent, or require retraining, which limits their use as systematic, reusable tools for evaluating internal robustness across architectures and domains. To overcome these limitations, this work proposes SYNAPSE, a systematic, training-free framework for understanding and stress-testing the internal behavior of Transformer models across domains. SYNAPSE extracts per-layer *[CLS]* representations, trains a lightweight linear probe to obtain global and per-class neuron rankings, and applies forward-hook interventions during inference. This design enables controlled, repeatable experiments on internal representations without altering the original model, thereby allowing weaknesses, stability patterns, and label-specific sensitivities to be measured and compared directly across tasks and architectures. Across all experiments, SYNAPSE reveals a consistent, domain-independent organization of internal representations, in which task-relevant information is encoded in broad, overlapping neuron subsets. This redundancy provides a strong degree of functional stability, while class-wise asymmetries expose heterogeneous specialization patterns and enable fine-grained, label-aware analysis. In contrast, small structured manipulations in weight or logit space are sufficient to redirect predictions, highlighting complementary vulnerability profiles and illustrating how SYNAPSE can guide the development of more robust and interpretable Transformer models.

Keywords: Interpretability, Robustness, Privacy, Model Auditing, Representation learning, Model Evaluation, Explainability

1. Introduction

With the rise of AI comes serious concerns about its reliability, trustworthiness, and robustness. As models become more complex, they become black boxes, making it difficult to understand how they reach their conclusions. In critical scenarios, such as medical diagnosis, military anti-missile systems, or malware detection, the inability to explain a decision can have catastrophic consequences. Explainable AI (XAI) seeks to shed light on internal processes and provide human-interpretable explanations, a crucial task as complexity grows and transparency is traded for high predictive performance [1]. While researchers have developed techniques to support validation and enhance robustness, most progress remains focused on Natural Language Processing (NLP) [2, 3]. Furthermore, increasing regulations and social concerns, such as the EU AI Act, drive interest in avoiding bias and ensuring fair interactions [4]. In recent years, advances in RNNs and LSTMs have enabled high-level performance, yet they face limitations in parallelization and in capturing long-range dependencies [5]. To overcome these, the Transformer architecture and its self-attention mechanism seek to determine which parts of the input data should be held in consider-

ation the most, giving more importance (or paying more attention) to the most relevant elements in a sequence [6]. This led to the development of Large Language Models (LLMs) such as GPT, BERT, and RoBERTa [7, 8, 9]. These models, pre-trained on massive datasets, can be fine-tuned for diverse tasks with relatively little data [8, 9]. Recently, this has been applied to cybersecurity, with studies showing that LLMs can achieve state-of-the-art results in malware detection using system call sequences [10]. Despite this progress, the application of XAI and robustness evaluation in the cybersecurity domain remains limited, a gap this work aims to address. Despite the growing body of work on neuron-level analysis, several limitations remain. Current approaches based on the representation erasure measure assess the impact of removing parts of the internal signal, but they operate as broad perturbation methods and do not provide a fine-grained mechanism to localize and manipulate individual functional units in a controlled, reusable manner [11]. Subsequent work demonstrated that specific neurons can be identified and even modified to influence model behavior; however, these methods typically rely on task-specific training procedures or architecture-dependent pipelines, which limit their applicability as general, training-free analysis tools [12]. Other studies have shown that high-level behaviors such as sentiment can emerge in individual units of generative models, yet these findings are largely observational and do not provide a systematic framework to measure robustness or to perform targeted interventions

*Corresponding author.

Email addresses: jesus.sanchezo@um.es (Jesús Sánchez Ochoa),
enriquetomas@um.es (Enrique Tomás Martínez Beltrán),
alberto.huertas@um.es (Alberto Huertas Celdrán)

without affecting the rest of the network [13]. More recently, empirical evidence suggests that task-relevant knowledge is often distributed across many neurons rather than isolated in a small subset, making it difficult to assess how internal representations contribute to model decisions using simple attribution or ablation strategies [14]. In addition, most neuron-level interpretability advances have been developed and evaluated in the context of Natural Language Processing, with comparatively little effort devoted to designing domain-independent methodologies that can be transferred across tasks and data modalities.

To address this gap, this work shifts from descriptive neuron analysis to a causal and operational perspective, in which internal units are systematically ranked and intervened at inference time to quantify their functional role. In this setting, neuron-level interpretability is not treated as a purely explanatory tool but as an experimental mechanism to assess robustness, sensitivity, and class-conditional behavior across architectures and domains. This objective is articulated through the following research questions:

- RQ1 Global sensitivity. How many top- k neurons must be silenced to impact overall performance across models and domains significantly?
- RQ2 Label-aware brittleness. Does silencing a small, label-aware subset of neurons meaningfully affect metrics tied to a target label?
- RQ3 Class-conditional vulnerability. Which labels are most sensitive to per-class neuron silencing, and does this pattern differ between malware and language domains?

To operationalize this causal, training-free analysis setting, this work introduces SYNAPSE, a framework for systematically analyzing and stress-testing the internal behavior of Transformer-based models across domains. Rather than providing purely descriptive explanations, SYNAPSE enables controlled, inference-time interventions that quantify the functional role of internal units in terms of robustness, sensitivity, and class-conditional behavior. Concretely, the contributions of this work are as follows:

- **SYNAPSE framework.** A modular and non-destructive pipeline that automatically extracts layer-wise [CLS] activations, trains lightweight linear probes to obtain global and class-conditional neuron importance rankings, and performs targeted interventions through forward hooks without retraining.
- **Causal silencing strategies for neuron-level robustness evaluation.** Three complementary intervention mechanisms are introduced: (i) *global undirected silencing*, which removes the top- k neurons according to a global ranking to measure overall sensitivity; (ii) *global directed silencing*, which selects globally important neurons with maximal influence on a target label to perform label-aware analysis; and (iii) *per-class silencing*, which suppresses neurons associated with a specific class to directly probe class-conditional brittleness.

- **Efficient and architecture-agnostic analysis.** The use of compact [CLS] representations enables a computationally efficient and scalable neuron-level pipeline applicable to different Transformer encoders.
- **Cross-domain experimental validation.** A unified evaluation protocol spanning malware detection from system-call sequences and emotion classification from natural language, allowing direct comparison of neuron-level behavior across heterogeneous modalities.

The remainder of this paper is organized to reflect the development of the proposed approach. Section 2 positions this work within the literature on neuron-level interpretability and adversarial analysis. Section 3 introduces the threat model that defines the realistic conditions under which training-free internal interventions are carried out. The design and components of the SYNAPSE framework are presented in Section 4. The experimental protocol, including datasets, evaluation metrics, and architectural settings, is detailed in Section 5. The results obtained across domains are reported and analyzed in Section 6. Finally, Section 7 discusses the main findings and limitations, and Section 8 concludes the paper and outlines future research directions.

2. Related Work

This section reviews recent work along two main research directions: (i) neuron-level explainable AI methods, which aim to identify and analyze neurons that encode class-specific information, and (ii) attacks on machine learning models, which study how targeted manipulations can induce misclassification. Table 1 and Table 2 provide a comparative taxonomy of representative methods across these two axes and serve as a structural reference for the subsequent subsections.

2.1. Explainable Artificial Intelligence

A trend in XAI techniques is to perform causal neuron analysis of the model, which involves actively intervening on neurons to test their effects on model behavior. The goal of these techniques is to identify important neurons by ablating or manipulating them and observing changes in their outputs, an approach adopted in this work. Li et al. [15] used this idea to understand neural network representations, removing neurons from RNNs to see the impact on translation accuracy, confirming that neurons indeed carried specific linguistic information. Afterwards, Bau et al. [12] expanded on this idea by identifying and directly controlling key neurons in a neural machine translation model, showing that activating or suppressing these neurons could modify specific behaviors. A different approach was presented in Radford et al. [16], which sought a single “sentiment neuron” that could alter the sentiment of generated text by adjusting its activation. Lastly, Song et al. [14] focused on neurons in LLMs that may be uniquely responsible for certain tasks and found that disabling them reduced task performance, confirming their causal role in those tasks. Together, these studies demonstrate that individual neurons can assume

causal, interpretable roles. However, they also reveal that scaling to larger architectures (e.g., LLMs) requires more systematic methods for locating and manipulating these causal units, a gap this work aims to fill.

Another line of work studies how individual neurons specialize in representing specific concepts within neural models. Early findings show that internal representations tend to organize into functional substructures, with different neurons capturing distinct linguistic properties such as sentiment, syntax, or semantics.

This idea is formalized through Linguistic Correlation Analysis, where simple probe models are trained on individual neuron activations to predict interpretable features and quantify neuron specialization. This approach was introduced by Dalvi et al. [17] and later extended by Durrani et al. [18]. Building on this methodology, Dalvi et al. also released NeuroX, a toolkit that provides modular support for neuron-level probing and remains one of the few frameworks explicitly designed to operate at this level of granularity [19].

2.2. Attacks on Machine Learning Models

In general, white-box evasion techniques assume the attacker has access to the full model, including gradients, training data, and model weights, making it easier to craft highly effective adversarial examples that can significantly degrade model precision. Firstly, Szegedy et al. [20] demonstrated that imperceptible, L-BFGS-optimized perturbations revealed deep networks' vulnerability to carefully crafted adversarial examples. Building on this, several authors have examined the impact of imperceptible input perturbations on misclassification in deep networks, as in Goodfellow et al. [21], who introduced FGSM (Fast Gradient Sign Method). This method uses the gradient to craft perturbations that maximize loss in a quick one-step attack. Further research by Pravin et al. [22] proposed a neuron-fragility-exploitation attack that identifies and perturbs a small set of highly sensitive neurons in ResNet models to induce misclassifications, an approach that motivates this thesis. Another important contribution was made by Che et al. [23], who extended white-box attacks to LLMs by manipulating latent and weight-space features. This precise category was chosen when this work was developed, as robustness can be measured with no extra effort when the model's critical data are available.

In conclusion, the reviewed literature shows that neuron-level analysis and adversarial robustness have largely evolved along separate paths. Existing interpretability methods successfully identify neurons with causal or specialized roles, but they are predominantly descriptive, strongly tied to NLP tasks, and lack a systematic and reusable protocol for large Transformer architectures. Furthermore, most adversarial approaches focus on input-space perturbations or direct weight manipulation, providing limited insight into how internal representations contribute to model stability or vulnerability. Moreover, current techniques rarely enable controlled, training-free interventions that can be consistently applied across domains and models. As a result, there is still no unified framework that enables the internal sources of robustness and fragility to be located, ranked, and

experimentally tested in a comparable, architecture-agnostic manner.

3. Threat Model

In the context of deploying LLMs in high-stakes domains such as cybersecurity and defense, this work considers a threat landscape in which models face not only input-level perturbations but also internal manipulation and operational degradation. The necessity for the SYNAPSE framework is motivated by several realistic threat scenarios that directly correspond to the neuron intervention strategies developed:

- **TH-1: Traffic evasion by mimicking legitimate behavior.** In real networks, attackers frequently adapt malicious communication to resemble normal traffic, for example, by blending command-and-control exchanges into common patterns that appear to be regular HTTPS or DNS traffic. The objective is straightforward: reduce the observable signals that security systems use to discriminate between malicious and benign activity, thereby increasing the probability that harmful traffic is accepted as normal.
- **TH-2: Compromised or altered model before deployment.** A separate and increasingly common risk is that the model itself is modified somewhere along the deployment pipeline, such as during training, packaging, storage, or distribution. In this scenario, the model appears to work correctly in routine use, but behaves incorrectly under attacker-chosen conditions, for instance, misclassifying a specific type of malicious activity while leaving other predictions largely unaffected. This kind of tampering can be subtle, difficult to detect, and operationally attractive because it preserves an appearance of normal performance.
- **TH-3: Faults that corrupt computation during inference.** Deployed systems may experience transient faults that do not change the input data but still perturb the internal computation, such as memory bit flips, hardware instability, or electromagnetic interference in edge or critical environments. Even when rare, these events can distort intermediate representations and lead to unreliable or unsafe decisions, particularly in settings where the classifier is part of an automated response pipeline.
- **TH-4: Manipulation of the serving process and final outputs.** If the inference service is compromised, an attacker may not need to alter inputs or model weights to influence decisions. Instead, they can directly steer predictions at the output stage, for example, by biasing scores toward the normal class or by altering the decision logic applied to logits. This scenario is particularly relevant in production deployments, where the model runs as a service and its outputs are consumed downstream by monitoring or mitigation components.

Table 1: Comparison of Neuron Analysis Methods.

Reference	Year	Model Type	Domain / Purpose	Explanation Type	Scope
Li et al. [15]	2017	LSTM-based NLP classifier	NLP (sentiment, linguistic tasks)	Feature ablation	Local Global
Radford et al. [16]	2017	mLSTM	NLP (unsupervised text generation)	Emergent feature analysis	Global
Bau et al. [12]	2019	NMT	NLP (machine translation)	Neuron importance ranking and manipulation	Global
Dalvi et al. [17]	2018	Pre-trained RNN	NLP (various language tasks)	Neuron interpretation	Global
Durrani et al. [18]	2020	Transformer (BERT)	NLP (language understanding)	Neuron importance and clustering	Global
Dalvi et al. [19]	2023	Transformers	NLP (interpretability)	Toolkit supporting multiple neuron analysis methods	Local Global
Song et al. [14]	2024	LLM	NLP (multi-task)	Causal analysis	Global

Table 2: Adversarial and poisoning attacks in machine learning.

Reference	Year	Threat Model	Attack Type	Phase	Access	Model Type
Szegedy et al. [20]	2014	Evasion	Small perturbation adversarial examples (L-BFGS method)	Inference	White-box	DNN (CNN)
Goodfellow et al. [21]	2015	Evasion	FGSM (Fast Gradient Sign Method)	Inference	White-box	DNN (CNN)
Pravin et al. [22]	2021	Evasion	Neuron-fragility exploitation (target-specific “fragile” neurons)	Inference	White-box	DNN (ResNet)
Che et al. [23]	2024	Capability elicitation	Hidden feature/weight manipulation (latent and weight-space attacks)	Inference (and fine-tune)	White-box	LLM (GPT family)

4. Synapse Framework

This section details the system design used to study neuron-level behavior and robustness. The framework comprises three blocks that orchestrate the analysis and intervention process: (i) Explainability Block, which extracts [CLS] activations layer-wise (i.e., the sequence-level representation used for classification) and trains a lightweight linear probe to quantify neuron importance; (ii) Analysis block, which converts probe weights into global and per-class rankings, mapping top- k neuron indices to specific layers and hidden dimensions to enable reproducible, scope-controlled interventions, carried out in the (iii) Adversarial block. In addition, it implements a variety of inference-time perturbations via PyTorch forward hooks, including global undirected, label-directed, and per-class silencing, as well as auxiliary stress tests such as logit bias, Gaussian noise, and weight-tilting. This modular, training-free, and reversible setup is illustrated in Figure 1, which shows the complete architecture of the framework.

This work is inspired by the approach developed in Dalvi et al. [24] and their NeuroX library, which served as the basis for activation extraction, probe training, and neuron importance computation. Nevertheless, these tools had to be adapted to meet the requirements of this work.

The framework operates as a cyclic workflow to ensure experimental integrity and reproducibility. Each execution follows a six-step protocol:

1. **Ranking:** Compute global and class-specific rankings on a held-out data split.
2. **Selection:** Identify the top- k indices based on the desired p and scope.

3. **Intervention:** Register PyTorch forward hooks to intercept and modify activations during inference.
4. **Inference:** Run the model on the test set and record performance metrics.
5. **Cleanup:** Remove all active hooks to restore the model to its original state.
6. **Verification:** Recompute the baseline to ensure no permanent changes were made to the weights.

This non-destructive intervention is made possible by forward hooks. In the PyTorch ecosystem, hooks are user-defined mechanisms registered with modules or tensors to enable the inspection, extraction, or modification of intermediate computations. They are triggered at specific stages of execution (such as the forward or backward pass) without altering the model’s underlying architecture. This allows the framework to dynamically register and unregister modifications as needed, ensuring that no permanent changes are made to the model’s weights. In this work, forward hooks are used to silence targeted neurons during inference, enabling stress testing of the model’s robustness in a reversible setup.

All parameters, including random seeds and the specific JSON-persisted neuron indices, are logged to guarantee that any intervention can be exactly replicated across both the malware and GoEmotions domains.

4.1. Explainability block

The Explainability Block is the foundational component of SYNAPSE, designed to map the model’s internal logic by quantifying the contribution of individual neurons to the classification task. This module performs a non-destructive extraction of internal activations (the numerical responses of neurons to

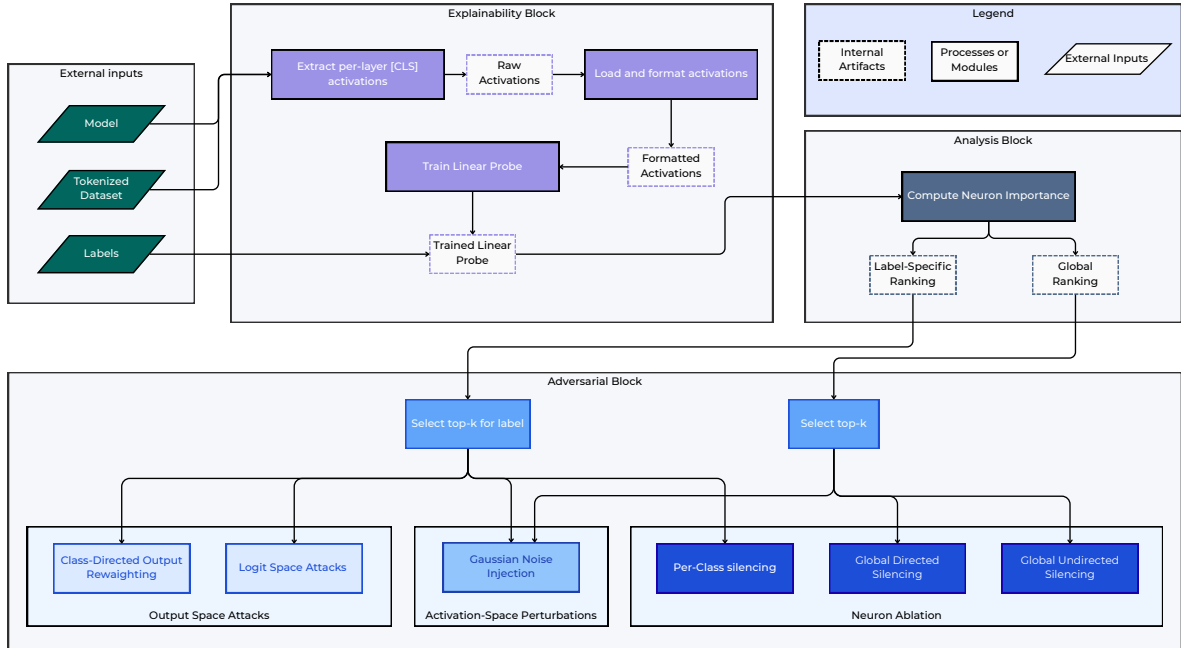


Figure 1: Internal structure of SYNAPSE

specific inputs to study how information is encoded across the transformer layers without altering the model’s parameters.

A critical technical element introduced at this stage is the [CLS] (Classification) token. In Transformer-based architectures, the [CLS] is a special token prepended to every input sequence. After passing through the encoder layers, the final hidden state is designed to serve as a summarized representation of the entire sequence for classification.

To validate the framework’s versatility across different domains, two distinct datasets are employed. First, a tokenized version of the **MalwSpecSys** dataset is used, containing system call sequences labeled as *Normal*, *Bashlite*, *Bdvl*, *Ransomware-PoC*, or *TheTick*. Second, the **GoEmotions** corpus is evaluated using a *monologg/bert-base-cased-goemotions-original* model, focused on a six-class slice: *anger*, *disgust*, *fear*, *joy*, *sadness*, and *surprise*.

The decision to extract activations exclusively from the [CLS] token is driven by computational efficiency. Due to the significant length of input sequences (particularly in system call traces, which can produce extremely long token sequences), extracting activations for every token would incur prohibitive computational costs and inefficient data management. By focusing on the [CLS] token at each encoder block, the framework achieves a drastic reduction in dimensionality and processing time. While this approach moves away from token-level granularity, the resulting summary preserves the global context needed for accurate, scalable neuron importance ranking, ensuring the analysis remains feasible even for large-scale models.

Activation Extractor. This block extracts the internal representations associated with the [CLS] token across all hidden layers of a Transformer model, serving as the basis for subsequent neuron-level analysis. First, each tokenized input is run through the model to extract the set of hidden states of every layer, apart from the embedding layer, which represents an initial representation of information and has no valuable information, and the last classification layer included in the model, which was discarded because of its obvious importance, presenting one neuron per label. When task-specific information is extracted from the remaining layers, the hidden states are stacked, and the [CLS] token is isolated for extraction.

Activation Loader. This module loads previously extracted neural activations from disk and prepares them for subsequent analysis. For each syscall sequence, it returns an activation matrix that can be used as input for probing classifiers and neuron-level analyzes.

Linear Probe Training. A linear probe, a simple linear classifier used to evaluate the information encoded in the representations of a pre-trained model, is trained to be applied on top of the frozen [CLS] representations and neither alters the original model nor is it a substitute for it. Instead, it verifies whether these representations encode features that can be separated by the linear classifier. Probe accuracy is a direct measure of how effectively the network has distilled input information into linearly separable patterns aligned with the target labels.

4.2. Analysis Block

After training the probing classifier, two custom functions were implemented to provide more control over neuron selection. The aim of these functions is to obtain:

- **A global ranking**, identifying most important neurons across all classes combined. This method computes a ranking of all neurons by the sum of their absolute weight contributions across classes, and selects the top- k neurons by count, where k is the number of neurons to be further silenced.
- **A label-specific ranking**, highlighting neurons particularly important for predicting each individual label. This approach computes importance weights independently for each output label, enabling a targeted selection of neurons.

These rankings guide the selection of neurons to silence during the experiments and enable a systematic evaluation of model robustness under various perturbation strategies.

Top-K Neuron Selection. To evaluate the impact of internal representations on model behavior, the framework must first identify which units are most functionally relevant.

Neuron Importance Estimation. Neuron importance is quantified using the weights of a lightweight linear probe trained on the [CLS] activations extracted from each encoder layer. The probe assigns a weight to each neuron for each output class, serving as a proxy for its contribution to the classification decision. Two types of importance rankings are derived from these weights:

- *Global ranking:* The importance of a neuron is defined as the sum of the absolute values of its weights across all classes, representing label-agnostic relevance.
- *Class-conditional ranking:* The importance is defined by the absolute value of the weight assigned to a specific class c , representing label-specific relevance.

Selection and Scope. Based on a selection percentage $p \in (0, 1]$, the framework identifies the top- k neurons to be targeted. The value of k depends on the chosen scope of the intervention:

$$k = \begin{cases} \lfloor p \cdot H \cdot L \rfloor & \text{for multi-layer scope} \\ \lfloor p \cdot H \rfloor & \text{for last-layer only scope} \end{cases} \quad (1)$$

where H represents the hidden size and L the number of layers. Global neuron indices are then mapped to their specific layer and local hidden dimension using integer division and modulo operations with respect to H .

4.3. Adversarial Block

This section describes the suite of perturbations implemented to evaluate the model’s internal resilience. The framework’s attack surface comprises several strategies designed to probe how information loss affects classification: (i) Silencing, which

mutes specific neurons to test functional redundancy; (ii) Noise Injection, which introduces stochastic perturbations; and (iii) Logit and Weight Manipulation, used for stress-testing under extreme conditions.

Silencing policy. Silencing sets the activations of selected dimensions to zero in the encoder output during the forward pass. This process is non-destructive and training-free: no gradients are computed, and no model parameters are permanently modified. The primary objective of the silencing policy is to identify the degree of functional specialization within the model’s architecture. By systematically muting neurons, one can determine whether specific labels depend on a small set of highly specialized units or whether task-relevant information is distributed across the network. Three silencing variants are implemented:

- **Global Undirected Silencing:** Targets the top- k neurons from the global ranking. The goal is to evaluate the model’s overall stability after removing its most active units across all classes.
- **Global Directed Silencing:** Selects neurons that have the strongest influence on a specific target label according to the linear probe, but applies a zeroing intervention. This tests the model’s ability to identify a particular class can be neutralized by silencing its most vocal supporters.
- **Per-Class Silencing:** Focuses exclusively on the top- k neurons belonging to a specific class’s ranking, probing class-conditional brittleness and potential leakage between labels.

Global Neuron Ablation Experiment (TH-3). The first type of experiment focused on the global importance of neurons. The top-ranked neurons across all classes were progressively silenced, starting with a small number of neurons and increasing incrementally. After each step, the model’s overall classification performance was evaluated to assess how performance degradation correlates with silencing key neurons.

Label-Specific Neuron Ablation Experiment (TH-3). The second type of experiment is focused on label-specific importance. For each label, neurons identified as most critical to that label were progressively silenced. After each ablation step, the model’s ability to correctly classify instances of that particular label was assessed, enabling a detailed analysis of the specialization and role of different neurons in the decision-making process.

Logit Bias (TH-4). This intervention perturbs the model outputs directly by adding a constant offset to the logit of a target class just before the softmax. Concretely, a forward hook is installed on the model’s output to add a bias b to the logit of class c^* at inference time (optionally, a balanced variant subtracts a small amount from the remaining classes to increase contrast). No parameters are trained or permanently modified; the change

is transient and removed after the run. This design emulates output-layer tampering used in white-box threat models while remaining architecture-agnostic and reversible. In this work, it is adapted to the neuron-centric setting by reporting how the induced shift interacts with the probe-driven class structure (e.g., the fraction of samples redirected to c^* and per-class F1-Score under attack).

Gaussian Noise (TH-3). This intervention injects zero-mean Gaussian noise into [CLS] activations of the encoder at selected neuron dimensions. Forward hooks are registered on the encoder’s output blocks; at each block, the [CLS] vector is perturbed at the top- k neuron indices provided by the probe ranking (global or class-conditional). The noise magnitude is governed by a standard deviation σ , and the scope can be last-layer only or all layers. Unlike classical baselines that add noise at the input embedding level, this variant places perturbations *inside* the network and guides them by attribution, emphasizing neurons deemed influential by the probe. The attack is fully training-free and reversible, and it allows controlled sweeps over (k, σ) to quantify robustness as a function of neuron importance.

Class-Directed Output Reweighting (TH-2). This intervention emulates weight-space tampering at inference time by temporarily editing the linear classification head. Let $W \in \mathbb{R}^{C \times H}$ and $b \in \mathbb{R}^C$ be the head’s weights and bias (from hidden size H to C classes). A copy of (W, b) is backed up; then, for a target class c^* , small increments Δ are applied only on the *columns* of W that correspond to the top- k neuron indices (global or class-conditional) mapped to hidden dimensions. Optionally, a balanced push reduces the same columns for non-target rows to enhance separation, and a selective suppression term can suppress a specific competitor class. A bias-only variant modifies b instead of W . After inference, the original parameters are restored. This design adapts ideas from weight or bit-level fault attacks to a controlled, attribution-guided, training-free setting: modifications are confined to the head, targeted to probe-selected columns, and are strictly temporary, enabling clean ablation studies without retraining.

Random Noise Injection (TH-1). As a baseline comparison, a simple random noise attack was implemented by directly adding noise to the model’s input embeddings. This method is not gradient-based and does not rely on the model’s internal computations. Instead, it introduces randomly generated perturbations to the input in an uninformed manner. This technique is commonly used in the literature as a baseline for evaluating model robustness [25, 26]. The intensity of the noise is controlled by a parameter epsilon (ϵ), which scales the amplitude of the random values added to each embedding vector. Higher values of ϵ lead to greater distortions and typically more severe performance degradation. In this work, noise was applied directly to the input embeddings during inference, without modifying the model’s parameters or input token sequence. For each input sequence, input embeddings are computed and perturbed by additive Gaussian noise scaled by a user-defined factor ϵ .

When Gaussian noise is injected into the embeddings, each token’s position in the original vector is shifted, subtly disrupting semantic relationships and the overall similarity structure among embeddings. As a result, the following layers receive distorted representations, leading to less coherent internal activations and, ultimately, reduced classification performance.

Fast Gradient Sign Method (TH-1). FGSM is a single-step adversarial attack proposed by Goodfellow et al. [21]. It works by adding a perturbation to the input in the direction of the loss function’s gradient, thereby maximizing the loss. This perturbation is scaled by a small factor ϵ that controls its magnitude. The lower the value of ϵ , the less perceptible the perturbation is. Unlike the random noise injection approach proposed in Subsection 4.3, which perturbs the input without considering the model’s behavior, FGSM generates targeted perturbations based on the model’s internal gradients, making it more effective and model-aware. To apply this approach to the scenario studied in this work, an FGSM variant was implemented and directly applied to the input embeddings of tokenized syscall traces. First, the cross-entropy loss is backpropagated to compute gradients with respect to each embedding vector. Then, a perturbation is created by taking the element-wise sign of that gradient and scaling it by a predefined ϵ to maximize loss. Finally, this signed perturbation is added to the original embeddings, yielding adversarial embeddings, which are then passed through the model to assess the resulting degradation in classification performance. The model is then tested with input examples to confirm the degradation, using state-of-the-art evaluation metrics.

5. Validation

A rigorous and reproducible evaluation protocol was established to ensure fair and meaningful comparisons across models, datasets, and experimental settings. The protocol standardizes data preprocessing, model configuration, and evaluation metrics, providing a consistent basis for analyzing the effects of neuron-level interventions under controlled conditions.

5.1. Experimental setup

Setting. The technical specifications of the machine used to run the experiments include an Apple M4 Pro chip and 24GB of RAM. The corresponding code for every described procedure is publicly available in [27].

Scenario. This work evaluates inference-time, white-box interventions at the neuron level (hidden representation dimensions) using PyTorch forward hooks. In this setting, an analyst has read-write access to intermediate activations during the forward pass but neither re-trains the model nor alters the training data.

Metric. The F1-Score was chosen as the primary evaluation metric because it balances precision and recall into a single value, ensuring that both false positives and false negatives are properly accounted for. More precisely, the macro-averaged F1-Score was used. By doing so, every label is given equal weight regardless of its support, ensuring that performance impact is measured consistently across all classes and preventing majority-class dominance from obscuring degradation in less frequent categories.

5.2. Experimental datasets

To evaluate the proposed approach across heterogeneous domains, experiments are conducted in two classification scenarios: malware detection from system-call sequences and emotion classification from natural-language text. These settings are selected to cover structurally diverse input modalities and tasks while relying on established, reproducible evaluation pipelines.

Malware detection. The malware experiments are based on the token-based detection pipeline introduced by Sánchez et al. [10], which models system-call traces as token sequences processed by a Transformer encoder followed by a linear classification head. This pipeline is adopted because it constitutes a well-established and validated baseline for sequence-based malware detection, enabling comparison with prior work while avoiding confounding architectural modifications.

The dataset consists of system-call sequences labeled as *Bashlite*, *Bdvl*, *Normal*, *RansomwarePoC*, and *TheTick*. The encoder architectures considered include *BERT*, *BigBird*, *DistilBERT*, and *Longformer*, covering both standard and long-sequence Transformer variants. The original model described in that work includes an additional final classification layer with one neuron per target class; this layer is excluded from the analysis, as directly manipulating output units would trivially affect predictions and would not provide insight into the internal representations learned by the encoder.

Emotion classification (GoEmotions). To complement the malware detection setting with a natural language task, experiments are also conducted on the GoEmotions dataset introduced by Demszky et al. [28], using the publicly available *monologg/bert-base-cased-goemotions-original* model. The GoEmotions dataset provides annotations for 28 emotion categories; to obtain a controlled and interpretable setting, a six-class subset consisting of *anger*, *disgust*, *fear*, *joy*, *sadness*, and *surprise* is constructed. Only single-label samples are retained, and the original 28-dimensional output logits are restricted to the selected classes, with predictions obtained by taking the argmax over this subset.

For controlled experimental sweeps, a stratified evaluation set balanced across classes is employed, with selected configurations replicated on larger batches when computational resources permit. Tokenization follows the original model tokenizer, using standard padding and truncation strategies.

5.3. Model representation choice

The selection of BERT-based architectures relies on the use of the [CLS] token, which serves as a condensed representation

Table 3: Architectural specifications of the evaluated Transformer models.

Model	Layers (L)	Hidden Size (d_{model})	Total Neurons (MLP)	Max. Seq. Length	Param. Count
BERT (base)	12	768	36,864	512	110M
BigBird	12	768	36,864	4,096	128M
DistilBERT	6	768	18,432	512	66M
Longformer	12	768	36,864	4,096	149M
GoEmotions (BERT)	12	768	36,864	512	110M

of the entire sequence’s contextual information. By focusing on the activations of the [CLS] token, the proposed framework significantly improves computational efficiency by avoiding the overhead of extracting data for each individual token while preserving the global features required for accurate neuron-level interpretability and classification analysis. Table 3

6. Results

This section presents a comprehensive evaluation of the experimental results obtained using the SYNAPSE framework. The analysis is structured into three main pillars: (i) Baseline Performance, establishing a reference for each architecture; (ii) Neuron-level Interventions, transitioning from global performance degradation to targeted class-specific silencing; and (iii) Comparative Stress-tests, where neuron-centric attacks are benchmarked against traditional gradient-based methods, noise injection, and weight-space manipulations. This progression enables characterization of how neuron importance, intervention scope, and domain-specific sensitivities influence the robustness of Transformer-based classifiers.

6.1. Malware Detection

This section presents the experimental results obtained with the proposed framework in the malware detection scenario, covering the different evaluation settings and intervention strategies considered in this study.

Before conducting any experiments, the baseline performance of the original models was evaluated using the MalwSpecSys dataset. As shown in Table 4, models designed to handle longer sequences, such as Longformer and BigBird, achieve the highest weighted F1-Scores (0.8516 and 0.8306, respectively). In contrast, BERT and DistilBERT perform worse, likely due to the fixed context window limitation when processing complex system call traces. These values provide a clean reference point for quantifying the degradation caused by subsequent silencing strategies.

6.1.1. Global Silencing

The first stage of the analysis considers Global Silencing, a class-agnostic approach that progressively disables a fixed proportion of the most salient neurons across the entire model. The objective is to assess the overall structural redundancy of the network: if performance drops sharply with minimal silencing, the model relies on a group of smart neurons, whereas if the drop is gradual, the knowledge is considered widely distributed.

Table 4: Baseline weighted F1-Score per model.

Model	Weighted F1-Score
BERT	0.6834
DistilBERT	0.6081
BigBird	0.8306
Longformer	0.8516
Baseline	0.8516

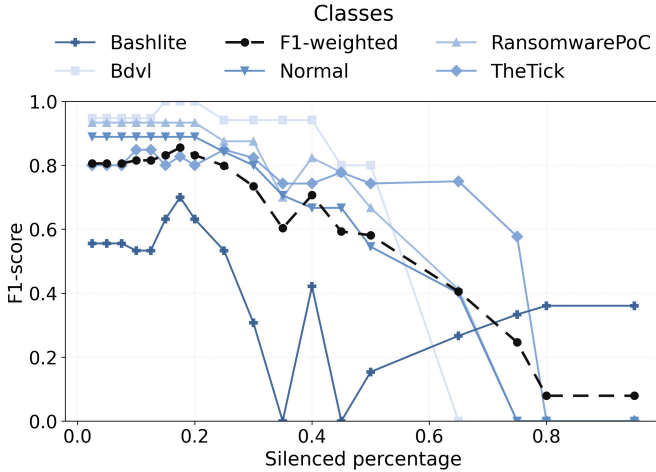


Figure 2: Global Silencing Attack results on BigBird

As seen in Figure 2, the hooks successfully intercepted the forward pass, leading to a noticeable and predictable degradation. When 50% of the most salient neurons are silenced, model performance nears a coin-flip scenario (0.5 F1-Score). It is observed that because only intermediate layers are targeted (leaving the final classification layer untouched), the degradation follows a gradual slope rather than an immediate collapse. This confirms that, although intermediate representations are critical, the final layer retains some discriminative power even under substantial internal noise. Table 5 provides a detailed comparison of this global attack across all tested architectures.

Figures 3a-3e show the F1-Score degradation (per target label) as progressively more salient neurons are silenced for each syscall traffic class. Across most targets, the curves drop by 50–60% (see, e.g., Figures 3a, 3b, and 3d), indicating that the model depends on relatively small subsets of neurons. In addition, while the F1-score for the targeted label decreases, other labels often degrade as well, and overall performance decreases (Figures 3a-3e), consistent with the distributed nature of the representations.

Looking at the raw activations extracted in the first section of the pipeline, the highest activations were around 0.6–0.7, and neurons showed positive activations for up to three different labels. This supports the idea that no tiny, fully isolated neuron groups can be identified for a more precise attack, and it also explains why other labels are affected when targeting a specific

one (Figures 3a-3e).

A particularly relevant case is *TheTick* (Figure 3c). Apart from being significantly affected when targeting other labels, silencing 40% of the top neurons associated with this label reduces its performance to 0, without noticeably harming the other traffic classes. This suggests that targeting the model components that drive decisions on *TheTick* could succeed in a real-world scenario while keeping other predictions largely intact (Figure 3c).

A similar pattern appears for *Bashlite* (Figure 3e), where attacking this label does not compromise normal traffic, which remains at F1-Score= 1.0; this would encourage the attack since usual traffic would continue to be classified normally (Figure 3e). Lastly, *RansomwarePoC* is comparatively robust against neuron-level attacks, as degrading its performance requires silencing a large number of neurons, and it also remains relatively stable when other labels are targeted (Figure 3b).

Across all Transformer models, class-targeted silencing produces highly asymmetric degradation patterns, indicating that each model exhibits localized, unevenly distributed class-specific sensitivities. Throughout analyzing collected data, three consistent trends emerge. The first one shows how **models differ sharply in their reliance on class-specialized neurons**. DistilBERT and Longformer frequently retain moderate performance for several labels even when the most influential neurons for that class are entirely suppressed (e.g., DistilBERT remains at F1-Score = 0.730 for Class-2; Longformer reaches F1-Score = 0.588 for the same class). In contrast, BERT and BigBird occasionally collapse to near-zero F1-Score for particular classes (e.g., BERT and BigBird both reach 0.000 for Class-2), indicating a more concentrated representation where a small set of neurons carries most of the discriminative power. Another shown trend shows that performance drops do not correlate uniformly with global model strength. Models with higher baselines (e.g., Longformer, BigBird) do not consistently show greater robustness. For example, BigBird (despite strong baseline performance) suffers dramatic collapses for several classes (F1-Score = 0.000 for Classes 2 and 4), suggesting that its high overall accuracy is supported by highly specialized neurons that, once removed, lead to brittle behaviour. Lastly, and being one of the main conclusions of this work, severe class-wise disparities reveal heterogeneous internal allocation of capacity. Furthermore, each model shows strong and weak classes. For example, BERT is resilient for Class-3 (F1-Score = 0.923) but fragile for Classes 0 and 2 (F1-Score = 0.167 and 0.000). In the case of DistilBERT collapses entirely for Class 3 but remains the most robust overall for Classes 0 and 2. Finally, BigBird is stable only for Class 1 and loses almost all discriminative ability for several others, while Longformer shows a relatively balanced degradation pattern but still exhibits strong asymmetry between classes.

Overall, these results indicate that class-specific neuron dependence is highly model-dependent and unevenly distributed, supporting the hypothesis that Transformer classifiers do not allocate representational capacity uniformly across labels. Instead, each architecture develops idiosyncratic islands of specialization, whose ablation exposes how the internal class struc-

Table 5: Global neuron silencing: weighted F1-Score for different Transformer models under increasing fractions of globally important neurons being silenced. $\Delta F1$ -Score denotes the relative variation with respect to the baseline.

Model	Baseline	5%	10%	20%	30%	50%	75%	95%	$\Delta F1@95\%$ (%)
BERT	0.683	0.686	0.686	0.686	0.686	0.575	0.482	0.147	-78.4
BigBird	0.785	0.806	0.815	0.832	0.735	0.581	0.246	0.079	-89.9
DistilBERT	0.608	0.608	0.608	0.608	0.608	0.608	0.499	0.311	-48.8
Longformer	0.852	0.844	0.871	0.852	0.768	0.535	0.097	0.079	-90.7

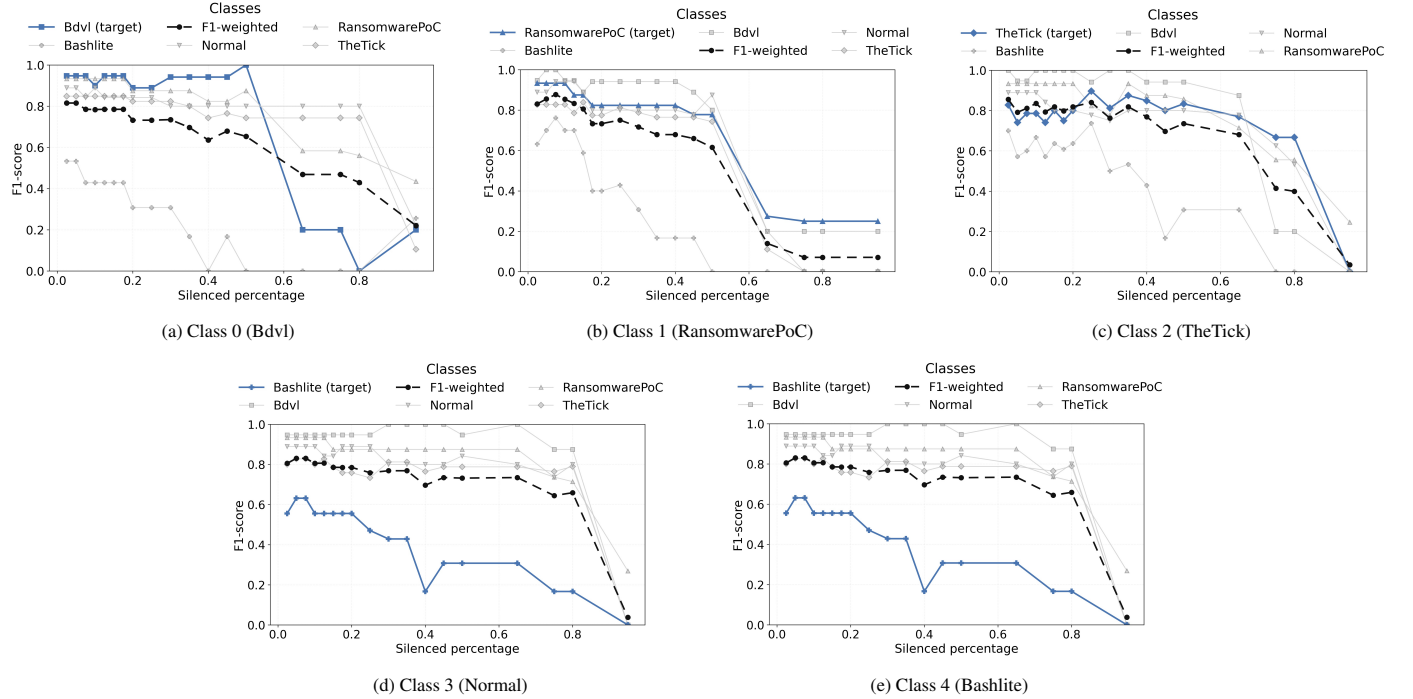


Figure 3: Results after silencing per-class ranking for BigBird across classes.

Table 6: Final performance under class-targeted neuron silencing (Classes 0–4).

Model	Class 0		Class 1		Class 2		Class 3		Class 4	
	F1	F1 WO*	F1	F1 WO						
BERT	0.167	0.166	0.800	0.528	0.000	0.242	0.923	0.455	0.533	0.328
BigBird	0.200	0.220	0.250	0.071	0.000	0.034	0.222	0.326	0.000	0.034
DistilBERT	0.444	0.212	0.909	0.348	0.730	0.489	0.000	0.481	0.182	0.195
Longformer	0.364	0.253	0.000	0.332	0.588	0.425	0.400	0.384	0.462	0.355

* WO: Weighted Overall.

ture emerges from a sparse subset of critical neurons.

6.1.2. FGSM Adaptation

In addition to neuron-level interventions, gradient-based attacks provide a complementary perspective on model vulnerability. In this context, the Fast Gradient Sign Method (FGSM) was adapted to operate under the constraints of the proposed framework, enabling a direct comparison between neuron-centric perturbations and gradient-driven attacks.

The FGSM results reveal a consistent monotonic degradation across all models as the perturbation strength increases.

Two global patterns. First, BERT and DistilBERT show the steepest declines, with their weighted F1-Score dropping by more than 20% at $\epsilon = 0.50$, indicating a high sensitivity to gradient-based perturbations injected at the input embedding level. Second, BigBird and Longformer exhibit smoother decay curves: even at a large perturbation budget (50%), both models retain F1 scores above 0.48 and 0.54, respectively, indicating greater inherent robustness. This divergence suggests that architectures designed for class separability, such as Longformer, develop more distributed and less brittle representations, whereas compact models relying on dense local interactions

Table 7: Impact of FGSM attack on model performance. The table reports the weighted F1-Score under different perturbation strengths, and the relative degradation compared to the baseline F1-Score.

Model	F1-Score (5%)	F1-Score (10%)	F1-Score (20%)	F1-Score (30%)	F1-Score (50%)	Δ F1-Score (%)
BERT	0.5121	0.4478	0.3952	0.3520	0.3015	-23.1%
DistilBERT	0.5013	0.4205	0.3667	0.3304	0.2801	-21.2%
BigBird	0.7310	0.6558	0.5887	0.5402	0.4814	-11.9%
Longformer	0.7702	0.7021	0.6504	0.5989	0.5407	-11.0%

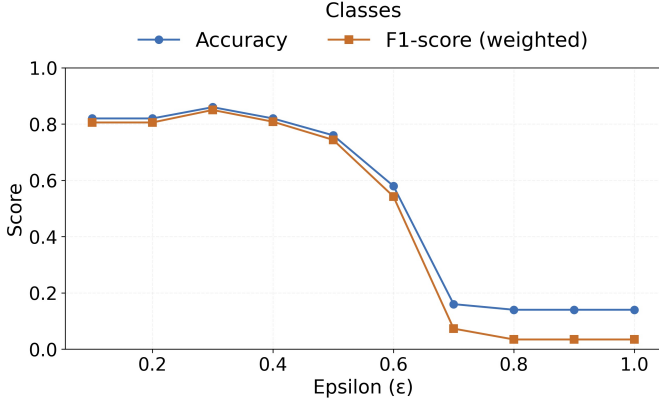


Figure 4: Random Noise model performance degradation

Table 8: Model robustness under random noise injection at different noise levels (ϵ).

Model	$\epsilon = 0.10$	$\epsilon = 0.50$	$\epsilon = 1.00$	Relative Δ F1-Score (%)
BERT	0.6081	0.6081	0.5214	-23.7%
DistilBERT	0.6081	0.6081	0.5214	-14.3%
BigBird	0.8306	0.8306	0.8306	0.0%
Longformer	0.8712	0.3903	0.0344	-95.9%

tions, such as BERT and DistilBERT, are more vulnerable to adversarial gradients that directly exploit the loss landscape.

6.1.3. Random Noise Injection

Random noise injection exposes markedly different robustness profiles across the four Transformer models. BigBird serves as an illustrative case through the sweep shown in Figure 4. For small perturbations ($\epsilon \leq 0.4$), both accuracy and weighted F1-Score remain essentially unchanged, oscillating around the baseline and indicating that BigBird is able to absorb low-magnitude unstructured perturbations at the embedding level. Once the perturbation exceeds a critical threshold ($\epsilon \approx 0.6$), performance collapses sharply: both metrics drop by more than half, and for higher noise levels ($\epsilon \geq 0.8$) the model enters a near-failure regime. This behaviour suggests that random perturbations disrupt the geometry of the embedding space only after a tipping point is reached, beyond which the internal attention structure can no longer maintain separability between classes.

The comparative results across models (see Table 8) show that this transition is highly model-dependent. Unexpectedly,

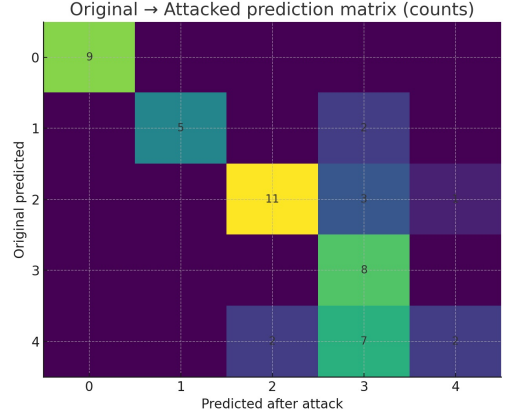


Figure 5: Logit Bias Attack results on BigBird

Table 9: **Logit Bias attack (bias = 8.0, target class = 3)**. Comparison across models based on accuracy, weighted F1-Score, percentage of predictions assigned to the target class, and percentage of flips from non-target classes.

Model	Accuracy	F1-Score (weighted)	% Pred. \rightarrow Target	% Flips (non-target)
BERT	0.7000	0.6867	40.00%	28.57%
BigBird	0.7200	0.7052	36.00%	28.13%
DistilBERT	0.6800	0.5896	18.00%	6.82%
Longformer	0.6400	0.6336	52.00%	42.86%

BigBird remains almost entirely unaffected, retaining its baseline F1-Score across all noise levels tested. BERT and DistilBERT show moderate degradation at high noise levels (-23.7% and -14.3%, respectively), indicating a less brittle but still noticeable sensitivity. Lastly, Longformer exhibits the most extreme behaviour: while stable at very low noise, it collapses almost entirely at $\epsilon = 1.0$ (F1-Score = 0.0344, a -95.9% drop). These divergent profiles suggest that robustness to uninformed noise is not directly correlated with baseline performance. Instead, it reflects architectural differences in how each model distributes semantic information across embedding dimensions.

6.1.4. Logit Bias

The logit-bias intervention produces a characteristic redistribution of predictions toward the target class $c^* = 3$, while preserving the overall structure of the classifier’s decision boundaries. Figure 5 shows the original \rightarrow attacked prediction mapping for BigBird under a bias of $b = 8$. The diagonal remains

Table 10: Performance under Gaussian Noise Injection ($\sigma = 0.9$, 60% of neurons perturbed).

Model	Weighted F1-Score
BERT	0.7421
DistilBERT	0.5812
BigBird	0.7624
Longformer	0.7443

partially intact, indicating that a subset of samples is robust to perturbations in the output layer. However, several off-diagonal blocks become populated, most notably the transitions $2 \rightarrow 3$ and $4 \rightarrow 3$, which reflect a systematic drift of multiple classes toward the target label. This behaviour is consistent with an additive shift applied directly to the output logits: classes with logits close to c^* are the first to flip. In contrast, well-separated classes remain stable unless the bias is sufficiently large.

The cross-model comparison in Table 9 shows that all architectures redirect a non-trivial fraction of predictions to the target class, but the intensity of this redirection varies markedly. DistilBERT is the most resistant, with only 18% of predictions assigned to the target and a low flip rate of 6.82%. In contrast, Longformer shows the strongest drift, with 52% of predictions redirected to the target and 42.86% of non-target samples flipping, suggesting a more compressible logit geometry. BERT and BigBird lie in an intermediate regime, exhibiting substantial but not catastrophic reweighting of outputs.

Overall, these results indicate that output-space manipulation induces structured, model-dependent distortions rather than uniform degradation. Because the intervention operates directly on logits without modifying hidden representations, the observed effects trace the intrinsic margin structure of each classifier: models whose logit distributions are tightly clustered around the decision boundaries are more susceptible to targeted shifts. At the same time, those with larger inter-class separations retain partial robustness even under strong bias.

6.1.5. Gaussian Noise Injection

The impact of Gaussian perturbations on the [CLS] representation is relatively mild across all models (see Table 10). Even with a high noise level ($\sigma = 0.9$) applied to 60% of the most influential neurons, the weighted F1-Scores remain close to their baselines, with no model experiencing severe degradation. At the same time, BigBird and Longformer maintain the highest robustness (F1-Score ≈ 0.76 and 0.74 , respectively), and DistilBERT shows the largest drop but still retains more than half of its predictive performance.

This pattern suggests that the models’ internal representations redundantly distribute semantic information across multiple neural dimensions, making them resilient to high-variance perturbations as long as the perturbations are zero-mean and unbiased. Unlike targeted manipulations (e.g., logit bias or weight-space attacks), Gaussian perturbations do not systemat-

Table 11: Balanced weight-push attack results.

Model	Accuracy	F1-Score (weighted)	Flips \rightarrow Target	Pred \rightarrow Target (%)
BERT	0.76	0.6834	2.27	14
BigBird	0.38	0.3126	71.43	76
DistilBERT	0.56	0.4151	18.18	28
Longformer	0.82	0.8073	0.00	6

Table 12: Class-suppression weight attack results.

Model	Accuracy	F1-Score (weighted)	Flips \rightarrow Target (%)	Pred \rightarrow Target
BERT	0.76	0.6834	2.27	14
BigBird	0.76	0.6741	14.29	28
DistilBERT	0.68	0.5871	4.55	16
Longformer	0.84	0.8315	0.00	6

Table 13: Bias-only weight attack results.

Model	Accuracy	F1-Score (weighted)	Flips \rightarrow Target (%)	Pred \rightarrow Target
BERT	0.76	0.6834	2.27	14
BigBird	0.82	0.8064	7.14	22
DistilBERT [†]	–	–	–	–
Longformer	0.86	0.8516	7.14	22

[†] DistilBERT is omitted because the probe assigned zero importance to all neurons, preventing the bias-only attack from being instantiated.

ically push predictions toward specific classes, which explains the relatively stable behaviour observed for all architectures.

6.1.6. Weights Targeted Attack

Balanced weight-push attack. This variant produces strong directional shifts in BigBird, which becomes highly susceptible to target-class redirection (76% of all predictions collapse to c^* , with 71.4% flips from non-target classes). In contrast, Longformer remains almost unchanged, indicating that its head weights are less aligned with probe-selected neurons and therefore more resilient. At the same time, BERT and DistilBERT exhibit moderate drift, suggesting partially concentrated but not overwhelmingly fragile weight structures. Table 11

Class-suppression weight attack. By explicitly weakening a single competitor class, this variant yields more controlled behaviour: BigBird exhibits reduced collapse relative to the balanced push, while Longformer remains stable. On the other hand, DistilBERT responds to suppression with small but noticeable increases in flips toward the target class, suggesting a more entangled, intermediate-level head geometry. Table 12

Bias-only weight attack. As expected, modifying only the bias vector produces the mildest effects. Models whose logits already provide clear inter-class separation (e.g., Longformer, BigBird) show minimal performance loss, whereas with BERT, the attack remains close to the baseline. Table 13

Overall, these results demonstrate that weight-space perturbations expose architecture-dependent vulnerabilities: BigBird is consistently the most vulnerable model, Longformer the most resistant, and BERT/DistilBERT occupy intermediate but distinct regimes. The contrast among variants also shows that attacks that modify the structure of W are far more damaging than those that affect only the biases, confirming that the head’s geometric configuration is a primary driver of robustness.

6.2. Emotion Detection

To complement the malware-oriented experiments, the framework is also evaluated on a fundamentally different domain: affective text classification. For this, this work employs the public monologg/bert-base-cased-goemotions-original model, trained on Google’s GoEmotions corpus [28]. As described in the experimental setup, the original 28-emotion space is reduced to a six-class configuration (anger, disgust, fear, joy, sadness, surprise). Only single-label examples are retained, and the model’s 28-dimensional output is remapped by restricting the logits to the six relevant indices and selecting the class with the highest score within this subset. A stratified and balanced mini-evaluation set is used to ensure stable estimation across perturbation sweeps.

While the malware experiments analyze each attack type in dedicated subsections, the GoEmotions case follows a different reporting strategy. Since the six-class model is not the focus of the interpretability study, which is a cross-domain stress test, the objective is to assess how the attacks generalize beyond system-call classifiers. For this reason, all neuron-level and weight-level perturbations are consolidated into a single summary table. This unified presentation simplifies cross-attack comparison, highlights global sensitivity trends, and avoids inflating the narrative with redundant per-attack subsections.

The resulting table shows the weighted F1-Score for each perturbation, along with the relative variation from the baseline. In addition, attacks operating in weight space report key behavioural effects (e.g., proportion of samples redirected to the target class), since in this domain such qualitative shifts can be more informative than the raw F1-Score score alone.

Table 14 summarizes the behavior of the GoEmotions model under the full set of neuron- and weight-level perturbations. As expected, the baseline achieves a high weighted F1-Score of 0.860, serving as a reference for the relative degradation observed across attacks.

Neuron-level attacks show heterogeneous effects. Global neuron silencing is the most disruptive intervention: removing 60% of neurons reduces performance to 0.300 (-65.1%), indicating a strong reliance on distributed representations. In contrast, per-class silencing behaves differently: targeting the neurons most associated with a specific emotion can improve the overall weighted F1-Score in certain configurations (peak 0.882, +2.6%), suggesting that the model contains redundancies or spurious correlations that can be moderated by selective ablations. Noise-based attacks produce intermediate degradation. Random noise injection yields 0.460 (-46.5%), while Gaussian noise ($\sigma = 0.9$) results in a softer drop to around 0.630

(-26.7%), reflecting a degree of robustness to smooth perturbations compared to discrete neuron removal.

Logit-space perturbations also exhibit notable sensitivity. The logit bias attack yields a stable $\Delta = 8$ (F1-Score = 0.624, -27.4%), whereas larger shifts collapse predictions almost entirely. This illustrates how small directional biases in the output layer can rapidly distort emotion predictions.

Weight-space attacks produce the most varied behaviours. The balanced weight push moderately harms performance (0.788, -8.4%), although qualitative effects such as increased redirection to the target class (16%) are more informative than F1-Score alone. The unbalanced push with suppression is substantially more aggressive, dropping the F1-Score to 0.492 (-42.8%) and misclassifying a large fraction (65%) of inputs into the target class. Conversely, the bias-only variant exhibits near-baseline behaviour (0.865, +0.6%), confirming that controlled modifications to the bias vector have limited global impact unless accompanied by changes to the weight matrix.

Overall, the GoEmotions experiments reveal a pattern consistent with the malware models: Global ablations and unstructured noise are highly damaging; selective manipulations can be either harmful or beneficial; and weight-space directional attacks provide powerful, configuration-dependent mechanisms for steering classifier behaviour.

7. Discussion

This section discusses the proposed training-free, neuron-level intervention framework and presents experimental results on malware detection and GoEmotions.

Across tasks and model architectures, the results consistently indicate that task-relevant information is distributed across broad and overlapping sets of neurons rather than concentrated in a small number of isolated units. Consequently, neuron-level interventions tend to produce gradual performance degradation, requiring increasingly large fractions of ablated neurons to induce substantial failures. At the same time, the analyses reveal architecture- and class-dependent sensitivities, where targeted interventions on specific neuron subsets can disproportionately affect certain decision pathways. These trends provide the basis for the discussion that follows.

A key strength of the framework is that it enables neuron-level analysis that is training-free, reversible, and model-agnostic. All interventions are performed at inference time via forward hooks, leaving model parameters unchanged and allowing immediate restoration after each run. By relying on [CLS] representations and a unified extraction procedure, the pipeline is consistent across BERT-like encoders and domains, enabling direct cross-domain comparisons. Methodologically, the framework treats explainability as a causal process: neuron importance is first estimated using a lightweight linear probe, and the same neurons are then intervened upon to verify their functional impact. This closes the gap between attribution and causation and yields quantitative robustness curves that relate performance degradation to the fraction of ablated neurons, both globally and per class. The design further emphasizes repro-

Table 14: Robustness of the GoEmotions model under neuron- and weight-level attacks (weighted F1-Score).

Attack	Config	F1-Score (weighted)	Δ F1-Score (%)
Baseline	–	0.860	–
Global neuron silencing	60% neurons silenced globally	0.300	-65.1
Per-class silencing	Best run (class 1), peak F1-Score = 0.882	0.882	+2.6
Random noise injection	$\epsilon = 1.5$ applied to top neurons	0.460	-46.5
Gaussian noise	$\sigma = 0.9$ (estimated)	0.630	-26.7
Logit bias	Best stable point ($\Delta = 8$). Higher Δ collapses predictions (F1-Score \downarrow to 0.192).	0.624	-27.4
Weight attack (balanced push)	$\Delta = 0.2$, $p = 20\%$, cols = 200. Flips \rightarrow target = 8 (16%). Overall predicted as target = 30%.	0.788	-8.4
Weight attack (unbalanced + suppression)	$\Delta = 0.5$, $p = 25\%$, suppress class 4. Flips \rightarrow target = 29 (58%). Overall predicted as target = 65%.	0.492	-42.8
Weight attack (bias-only)	$\Delta = 0.6$, bias-only adjustment. Flips \rightarrow target = 1. Stable behaviour (near-baseline).	0.865	+0.6

ducibility through controlled sweeps, explicit logging of neuron indices and layer scopes, and systematic checks of baseline recovery. Plus, to our knowledge, in the context of neuron-level robustness for cybersecurity and language under a single framework, this is one of the first pipelines that unifies explainability and adversarial-style interventions (via systematic silencing/attenuation) to reveal concrete failure budgets-how much targeted ablation is needed before performance breaks.

At the same time, the results reveal several limitations. In many cases, large fractions of neurons must be silenced to match the effect of simple input-space perturbations, underscoring the intrinsic robustness of the evaluated models to localized neuron ablations and the distributed nature of their internal representations. The current implementation focuses exclusively on [CLS] representations for tractability, omitting token-level structure and attention pathways that may influence certain behaviors. In addition, the reliance on a linear probe assumes approximate linear separability, and alternative attribution methods could alter neuron rankings and sensitivity profiles. From a validity perspective, the evaluation relies on publicly available checkpoints and controlled experimental settings; extending the analysis to broader datasets, additional architectures, and more diverse conditions would further strengthen these findings.

8. Conclusions and Future Work

This work presents SYNAPSE, a framework for analyzing neuron-level interpretability and robustness in Transformer-based models. By extracting per-layer [CLS] activations, ranking neurons globally and per class, and applying fine-grained perturbations via forward hooks, SYNAPSE provides a unified methodology to analyze how models structure task-relevant information and respond to controlled interventions. Experimental results reveal a consistent, domain-independent trend: Transformer models distribute information across broad, overlapping neuron subsets rather than concentrating it in isolated units, introducing internal redundancy that makes neuron-level attacks more costly than expected. At the same time, the framework reveals structural weaknesses in each architecture, in which

certain decision pathways are disproportionately sensitive to targeted perturbations, indicating non-uniform internal organization and reliance on narrow activation patterns. Complementary manipulations in logit space and weight space further show that small, structured changes can redirect predictions with minimal global degradation, highlighting attack surfaces not captured by neuron-centric analysis alone. Overall, the findings show that SYNAPSE supports interpretable inspection of internal representations and acts as a practical tool for stress-testing robustness in both cybersecurity and NLP applications.

Future work may extend SYNAPSE by developing neuron-level defense mechanisms that detect or mitigate targeted manipulations in realistic, security-critical deployments. Additional directions include exploring multimodal and cross-domain scenarios, where neuron attribution patterns may differ across textual, behavioral, and sensory inputs, and integrating interactive visualization tools to improve accessibility. Finally, deploying the framework in federated or distributed learning settings could provide insights into neuron-level robustness when models are trained collaboratively across heterogeneous devices and threat landscapes.

Acknowledgment

This work was supported by (a) MCIN/AEI/10.13039/50110 0011033/FEDER under grant PID2021-122466OB-I00, and (b) the Swiss Federal Office for Defense Procurement (armasuisse) with the TITAN project.

References

- [1] C. Rudin, Stop explaining black box machine learning models for high stakes decisions and use interpretable models instead, *Nature Machine Intelligence* 1 (5) (2019) 206–215. doi:10.1038/s42256-019-0048-x.
- [2] A. B. Arrieta, N. Díaz-Rodríguez, J. D. Ser, A. Bennetot, S. Tabik, A. Barbado, S. García, S. Gil-López, D. Molina,

- R. Benjamins, R. Chatila, F. Herrera, Explainable artificial intelligence (xai): Concepts, taxonomies, opportunities and challenges toward responsible AI, *Information Fusion* 58 (2020) 82–115. doi:10.1016/j.inffus.2019.12.012.
- [3] M. Danilevsky, K. Qian, R. Aharonov, Y. Katsis, B. Kawas, P. Sen, A survey of the state of explainable AI for natural language processing, in: *Proceedings of the 1st Conference of the Asia-Pacific Chapter of the Association for Computational Linguistics and the 10th International Joint Conference on Natural Language Processing*, Association for Computational Linguistics, Suzhou, China, 2020, pp. 447–459. doi:10.18653/v1/2020.acl-main.46.
- [4] European Parliament and Council, Regulation (eu) 2024/1689 of 13 June 2024 establishing harmonised rules on artificial intelligence (ai act), *Official Journal of the European Union*, eUR-Lex (2024).
- [5] K. Cho, B. van Merriënboer, D. Bahdanau, Y. Bengio, On the properties of neural machine translation: Encoder-decoder approaches, in: *Proceedings of SSST-8, Eighth Workshop on Syntax, Semantics and Structure in Statistical Translation*, 2014, pp. 103–111. doi:10.3115/v1/W14-4012.
- [6] A. Vaswani, N. Shazeer, N. Parmar, J. Uszkoreit, L. Jones, A. N. Gomez, Ł. Kaiser, I. Polosukhin, Attention is all you need, *Advances in neural information processing systems* 30 (2017).
- [7] T. B. Brown, B. Mann, N. Ryder, M. Subbiah, J. Kaplan, P. Dhariwal, A. Neelakantan, P. Shyam, G. Sastry, A. Askell, et al., Language models are few-shot learners, in: *Advances in Neural Information Processing Systems*, Vol. 33, 2020, pp. 1877–1901.
- [8] J. Devlin, M. Chang, K. Lee, K. Toutanova, BERT: Pre-training of deep bidirectional transformers for language understanding, in: *Proceedings of NAACL-HLT 2019*, 2019, pp. 4171–4186.
- [9] Y. Liu, M. Ott, N. Goyal, J. Du, M. Joshi, D. Chen, O. Levy, M. Lewis, L. Zettlemoyer, V. Stoyanov, Roberta: A robustly optimized BERT pretraining approach, *arXiv preprint arXiv:1907.11692* (2019). doi:10.48550/arXiv.1907.11692.
- [10] P. M. Sánchez Sánchez, A. H. Celdrán, G. Bovet, G. M. Pérez, Transfer learning in pre-trained large language models for malware detection based on system calls, in: *MILCOM 2024 - 2024 IEEE Military Communications Conference (MILCOM)*, 2024, pp. 853–858. doi:10.1109/MILCOM61039.2024.10773857.
- [11] J. Li, W. Monroe, D. Jurafsky, Understanding neural networks through representation erasure (2016). *arXiv:1612.08220*, doi:10.48550/arXiv.1612.08220. URL <https://arxiv.org/abs/1612.08220>
- [12] A. Bau, Y. Belinkov, H. Sajjad, N. Durrani, F. Dalvi, J. Glass, Identifying and controlling important neurons in neural machine translation, *arXiv preprint arXiv:1811.01157* (2018).
- [13] A. Radford, R. Józefowicz, I. Sutskever, Learning to generate reviews and discovering sentiment (2017). *arXiv:1704.01444*, doi:10.48550/arXiv.1704.01444. URL <https://arxiv.org/abs/1704.01444>
- [14] R. Song, S. He, S. Jiang, Y. Xian, S. Gao, K. Liu, Z. Yu, Does large language model contain task-specific neurons?, in: *Proceedings of the 2024 Conference on Empirical Methods in Natural Language Processing*, 2024, pp. 7101–7113. doi:10.18653/v1/2024.emnlp-main.403.
- [15] J. Li, W. Monroe, D. Jurafsky, Understanding neural networks through representation erasure, *arXiv preprint arXiv:1612.08220* (2017). doi:10.48550/arXiv.1612.08220.
- [16] A. Radford, R. Józefowicz, I. Sutskever, Learning to generate reviews and discovering sentiment, *arXiv preprint arXiv:1704.01444* (2017). doi:10.48550/arXiv.1704.01444.
- [17] F. Dalvi, N. Durrani, H. Sajjad, Y. Belinkov, A. Bau, J. Glass, What is one grain of sand in the desert? analyzing individual neurons in deep nlp models, in: *Proceedings of the AAAI Conference on Artificial Intelligence*, Vol. 33, 2019, pp. 6309–6317.
- [18] N. Durrani, H. Sajjad, F. Dalvi, Y. Belinkov, Analyzing individual neurons in pre-trained language models, in: *Proceedings of the 2020 Conference on Empirical Methods in Natural Language Processing (EMNLP)*, 2020, pp. 4865–4880. doi:10.18653/v1/2020.emnlp-main.395.
- [19] F. Dalvi, H. Sajjad, N. Durrani, NeuroX library for neuron analysis of deep NLP models, in: D. Bollegala, R. Huang, A. Ritter (Eds.), *Proceedings of the 61st Annual Meeting of the Association for Computational Linguistics (Volume 3: System Demonstrations)*, Association for Computational Linguistics, Toronto, Canada, 2023, pp. 226–234. doi:10.18653/v1/2023.acl-demo.21. URL <https://aclanthology.org/2023.acl-demo.21/>
- [20] C. Szegedy, W. Zaremba, I. Sutskever, J. Bruna, D. Erhan, I. Goodfellow, R. Fergus, Intriguing properties of neural networks (2014). *arXiv:1312.6199*, doi:10.48550/arXiv.1312.6199. URL <https://arxiv.org/abs/1312.6199>
- [21] I. J. Goodfellow, J. Shlens, C. Szegedy, Explaining and harnessing adversarial examples (2015). *arXiv:1412.6572*, doi:10.48550/arXiv.1412.6572. URL <https://arxiv.org/abs/1412.6572>

- [22] C. Pravin, I. Martino, G. Nicosia, V. Ojha, Adversarial robustness in deep learning: attacks on fragile neurons, in: International Conference on Artificial Neural Networks, Springer, 2021, pp. 16–28.
- [23] Z. Che, S. Casper, R. Kirk, A. Satheesh, S. Slocum, L. E. McKinney, R. Gandikota, A. Ewart, D. Rosati, Z. Wu, Z. Cai, B. Chughtai, Y. Gal, F. Huang, D. Hadfield-Menell, Model tampering attacks enable more rigorous evaluations of LLM capabilities (2025). `arXiv:2502.05209`.
URL <https://arxiv.org/abs/2502.05209>
- [24] F. Dalvi, H. Sajjad, N. Durrani, Neurox: A library for neuron analysis of deep nlp models, in: Proceedings of the 61st Annual Meeting of the Association for Computational Linguistics (Volume 3: System Demonstrations), Association for Computational Linguistics, 2023, pp. 226–234. doi:10.18653/v1/2023.acl-demo.21. URL <https://aclanthology.org/2023.acl-demo.21/>
- [25] Z. Zhao, D. Dua, S. Singh, Generating natural adversarial examples, arXiv preprint arXiv:1710.11342 (2017).
- [26] W. Xu, D. Evans, Y. Qi, Feature squeezing: Detecting adversarial examples in deep neural networks, arXiv preprint arXiv:1704.01155 (2017).
- [27] kikaymusic, Neuron-level interpretability and robustness in llms (code repository), <https://github.com/kikaymusic/Neuron-Level-Interpretability-and-Robustness-in-LLMs>, gitHub repository (2025).
- [28] D. Demszky, D. Movshovitz-Attias, J. Ko, A. Cowen, G. Nemade, S. Ravi, GoEmotions: A dataset of fine-grained emotions, in: Proceedings of the 58th Annual Meeting of the Association for Computational Linguistics (ACL), 2020, pp. 4040–4054. doi:10.18653/v1/2020.acl-main.372.